Journal of Solid State Chemistry 182 (2009) 2261–2268

Contents lists available at ScienceDirect

Journal of Solid State Chemistry

journal homepage: www.elsevier.com/locate/jssc

Synthesis and characterization of $La_{0.8}Sr_{1.2}Co_{0.5}M_{0.5}O_{4-\delta}$ (M = Fe, Mn)

H. El Shinawi [a], J.F. Marco [c], F.J. Berry [a,b], C. Greaves [a,*]

[a] School of Chemistry, University of Birmingham, Birmingham B15 2TT, UK
[b] Department of Chemistry, The Open University, Milton Keynes MK7 6AA, UK
[c] Instituto de Quimica-Fisica "Rocasolano", Consejo Superior de Investigaciones Cientificas, Serrano 119, 28006 Madrid, Spain

ARTICLE INFO

Article history:
Received 1 April 2009
Received in revised form
3 June 2009
Accepted 6 June 2009
Available online 12 June 2009

Keywords:
Ruddlesden–Popper
Oxygen-deficient
Neutron powder diffraction
Mössbauer spectroscopy
Magnetic order

ABSTRACT

The M^{4+}-containing K_2NiF_4-type phases $La_{0.8}Sr_{1.2}Co_{0.5}Fe_{0.5}O_4$ and $La_{0.8}Sr_{1.2}Co_{0.5}Mn_{0.5}O_4$ have been synthesized by a sol–gel procedure and characterized by X-ray powder diffraction, thermal analysis, neutron powder diffraction and Mössbauer spectroscopy. Oxide ion vacancies are created in these materials via reduction of M^{4+} to M^{3+} and of Co^{3+} to Co^{2+}. The vacancies are confined to the equatorial planes of the K_2NiF_4-type structure. A partial reduction of Mn^{3+} to Mn^{2+} also occurs to achieve the oxygen stoichiometry in $La_{0.8}Sr_{1.2}Co_{0.5}Mn_{0.5}O_{3.6}$. $La_{0.8}Sr_{1.2}Co_{0.5}Fe_{0.5}O_{3.65}$ contains Co^{2+} and Fe^{3+} ions which interact antiferromagnetically and result in noncollinear magnetic order consistent with the tetragonal symmetry. Competing ferromagnetic and antiferromagnetic interactions in $La_{0.8}Sr_{1.2}Co_{0.5}Fe_{0.5}O_4$, $La_{0.8}Sr_{1.2}Co_{0.5}Mn_{0.5}O_4$ and $La_{0.8}Sr_{1.2}Co_{0.5}Mn_{0.5}O_{3.6}$ induce spin glass properties in these phases.

1. Introduction

The recent interest in oxides with a K_2NiF_4-type structure is, in part, associated with their importance as models for understanding physical properties such as superconductivity and magnetoresistance. Additionally, K_2NiF_4-type phases such as $La_2NiO_{4+\delta}$ have recently attracted considerable interest as alternative materials for solid oxide fuel cells due to their interesting transport properties [1,2]. As $n = 1$ members of the Ruddlesden–Popper phases, the K_2NiF_4-type oxides have shown an enhanced stability under reducing conditions due to their ability to accommodate a wide range of coordination environments and oxidation states. Ruddlesden–Popper phases such as $Sr_3Fe_2O_{7-\delta}$ [3] and $Sr_{3-x}La_xFe_{2-y}Co_yO_{7-\delta}$ [4] have shown a high degree of structural stability in reducing environments at elevated temperature and reasonably good transport properties making them possible candidates for oxygen separation membranes and solid oxide fuel cells. We have previously shown that $LaSrCo_{0.5}Fe_{0.5}O_4$ is able to withstand reducing condition (10% H_2/N_2) up to 1000 °C via reduction of Co^{3+} to Co^{2+} and formation of $LaSrCo_{0.5}Fe_{0.5}O_{3.75}$ [5]. The oxide ion vacancies were disordered and distributed within the equatorial planes of the structure. In an attempt to characterize M^{4+}-containing phases, we have now synthesized the materials $La_{0.8}Sr_{1.2}Co_{0.5}Fe_{0.5}O_4$ and $La_{0.8}Sr_{1.2}Co_{0.5}Mn_{0.5}O_4$ as precursors to phases with higher degrees of oxygen deficiency and structural stability under reducing conditions. In particular, we show here that $La_{0.8}Sr_{1.2}Co_{0.5}Mn_{0.5}O_4$ is able to sustain an oxygen content as low as $O_{3.6}$ with retention of crystal symmetry when heated in 10% H_2/N_2 at 1000 °C. We present in this work the synthesis and characterization of $La_{0.8}Sr_{1.2}Co_{0.5}Fe_{0.5}O_4$ and $La_{0.8}Sr_{1.2}Co_{0.5}Mn_{0.5}O_4$ and of their reduced forms $La_{0.8}Sr_{1.2}Co_{0.5}Fe_{0.5}O_{3.65}$ and $La_{0.8}Sr_{1.2}Co_{0.5}Mn_{0.5}O_{3.6}$.

2. Experimental

The materials $La_{0.8}Sr_{1.2}Co_{0.5}Fe_{0.5}O_4$ and $La_{0.8}Sr_{1.2}Co_{0.5}Mn_{0.5}O_4$ were synthesized by a sol–gel procedure. Stoichiometric amounts of La_2O_3, $SrCO_3$, $Co(CH_3COO)_2 \cdot 4H_2O$ and $Fe(CH_3COO)_2$/$Mn(CH_3COO)_2 \cdot 4H_2O$ were dissolved in acetic acid and boiled under reflux for 3 h. Small amounts of hydrogen peroxide and water were added and the mixture was further refluxed overnight to obtain a clear solution. This solution was evaporated to a dark red gel in the case of $La_{0.8}Sr_{1.2}Co_{0.5}Fe_{0.5}O_4$ and a dark violet gel in the case of $La_{0.8}Sr_{1.2}Co_{0.5}Mn_{0.5}O_4$. The gel was dried and decomposed in air at 400 °C and the resulting powder pressed into pellets and calcined in flowing oxygen at 1350 °C for 18 h. The oxygen deficient materials ($La_{0.8}Sr_{1.2}Co_{0.5}Fe_{0.5}O_{3.65}$ and $La_{0.8}Sr_{1.2}Co_{0.5}Mn_{0.5}O_{3.6}$) were obtained by reducing the as-prepared materials in flowing 10% H_2/N_2 for 12 h at 700 and 1000 °C, respectively.

X-ray powder diffraction (XRD) data were collected using a Siemens D5000 diffractometer in transmission mode, employing Cu$K\alpha_1$ radiation from a germanium monochromator. Thermogravimetric analysis was performed using a Rheometric Scientific STA 1500 thermal analyzer where samples (~30 mg) were

* Corresponding author.
E-mail address: c.greaves@bham.ac.uk (C. Greaves).

0022-4596/$ - see front matter © 2009 Elsevier Inc. All rights reserved.
doi:10.1016/j.jssc.2009.06.010

reduced at 10 °C/min in 10% H_2/N_2. Neutron powder diffraction (NPD) data were collected at room temperature and 1.5 K on the HRPT diffractometer at SINQ, PSI using wavelengths of 1.8852 and 1.4942 Å. Rietveld refinements were performed on the powder diffraction data using the GSAS suite of programs [6] employing a pseudo-Voigt profile function. A correction for preferred orientation along the [001] direction was allowed in the refinement. Magnetic data were collected using a Quantum Design MPMS SQUID magnetometer in the temperature range 5–300 K. Zero-field-cooled (ZFC) and field-cooled (FC) data were collected on warming using an applied field of 0.5 T. The ac susceptibility was measured by varying the frequency from 30 Hz to 1 kHz with the field amplitude of 3 Oe. ^{57}Fe Mössbauer spectra were recorded at 298 and 16 K in constant acceleration mode using a ca. 25 mCi 57Co/Rh source and a helium closed-cycle cryorefrigerator. All the spectra were computer fitted and the chemical isomer shift data are quoted relative to metallic iron at room temperature.

3. Results

3.1. Structural characterization

XRD patterns showed the as-prepared and the reduced materials to be single-phase with no evidence of starting materials or product impurities. The patterns were indexed on a body-centred tetragonal unit cell related to a K_2NiF_4-type structure (Fig. 1). Structural refinements of the XRD data were performed employing the ideal tetragonal *I*4/*mmm* space group; however, as expected for X-ray diffraction data from materials of this type, the refinements were insensitive to oxide ion site occupancy. Oxide ion sites were therefore fixed at full occupancy in all samples and the refined unit cell parameters are given in Table 1.

The reduction behaviour of the as-prepared materials was followed by thermogravimetric measurements in which the materials were heated (10 °C/min) in flowing 10% H_2/N_2 (Fig. 2). The measurements suggest that, assuming the as-prepared materials are stoichiometric in oxygen, the reduced materials at 700 °C have very similar oxygen contents: $La_{0.8}Sr_{1.2}Co_{0.5}M_{0.5}O_{3.65}$. $La_{0.8}Sr_{1.2}Co_{0.5}Fe_{0.5}O_4$ undergoes slight decomposition due to separation of La_2O_3 (as indicated by XRD) at $T>800$ °C; however, $La_{0.8}Sr_{1.2}Co_{0.5}Mn_{0.5}O_4$ undergoes further reduction as the temperature increases and reaches the stoichiometry $La_{0.8}Sr_{1.2}Co_{0.5}Mn_{0.5}O_{3.6}$ at 1000 °C.

NPD data were collected from the reduced materials ($La_{0.8}Sr_{1.2}Co_{0.5}Fe_{0.5}O_4$ reduced at 700 °C and $La_{0.8}Sr_{1.2}Co_{0.5}Mn_{0.5}O_4$ reduced at 1000 °C) at room temperature to confirm oxygen stoichiometries suggested by TG analysis and to determine the oxide ion vacancy distribution in these materials. Rietveld profile refinements of the NPD data were performed adopting the *I*4/*mmm* space group. Profile fits and difference patterns are shown in Fig. 3; structural data and some selected bond lengths are given in Tables 2 and 3, respectively.

The NPD data were in good agreement with the TG results showing the overall stoichiometries of the reduced materials as $La_{0.8}Sr_{1.2}Co_{0.5}Fe_{0.5}O_{3.67}$ and $La_{0.8}Sr_{1.2}Co_{0.5}Mn_{0.5}O_{3.60}$. The results are therefore consistent with the view that the as-prepared materials are stoichiometric in oxygen, and the oxygen-deficient materials are, within experimental error, $La_{0.8}Sr_{1.2}Co_{0.5}Fe_{0.5}O_{3.65}$ and $La_{0.8}Sr_{1.2}Co_{0.5}Mn_{0.5}O_{3.6}$.

Refinements showed no evidence of symmetry lowering due to cation or vacancy order. The scattering length contrast in Co/Mn and Co/Fe is such that ordering would have been easily detected [7]. The oxide ion vacancies created in these materials are confined to the equatorial planes of the K_2NiF_4-type structure. Attempts to refine a model in which oxide ion vacancies were distributed between axial and equatorial positions in a manner similar to $NdSrCuO_{3.56}$ [8] proved unstable. A displacement of equatorial oxygens (O1) in the *xy* plane was also observed, which transforms the oxide ion at (0.5, 0, 0) to the split position (0.5, *y*, 0). The retention of the tetragonal symmetry under reduction with an equatorial distribution of oxide ion vacancies has been observed in related K_2NiF_4-type phases such as $LaSrCoO_{3.5+x}$ [9] and $La_{1+x}Sr_{1-x}C_{0.5}Fe_{0.5}O_{4-\delta}$ [5].

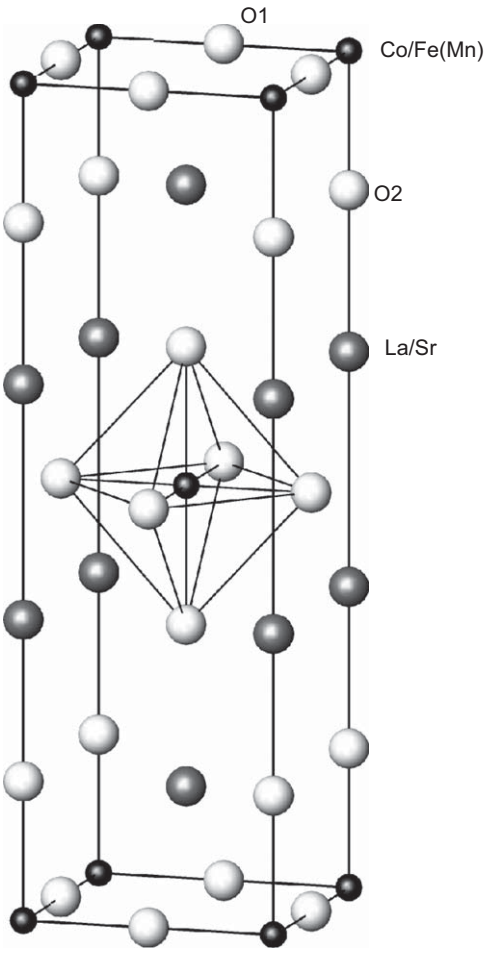

Fig. 1. Crystal structure of $La_{0.8}Sr_{1.2}Co_{0.5}M_{0.5}O_{4-\delta}$.

Table 1
XRD refined parameters for different samples.

Material	*a* (Å)	*c* (Å)
$La_{0.8}Sr_{1.2}Co_{0.5}Fe_{0.5}O_4$	3.82509(4)	12.5598(2)
$La_{0.8}Sr_{1.2}Co_{0.5}Fe_{0.5}O_{3.65}$	3.77148(9)	12.9725(4)
$La_{0.8}Sr_{1.2}Co_{0.5}Mn_{0.5}O_4$	3.83073(7)	12.5124(3)
$La_{0.8}Sr_{1.2}Co_{0.5}Mn_{0.5}O_{3.6}$	3.77928(3)	12.9802(1)

3.2. Mössbauer spectroscopy

The ^{57}Fe Mössbauer spectra recorded from $La_{0.8}Sr_{1.2}Co_{0.5}Fe_{0.5}O_4$ are shown in Fig. 4a. The ^{57}Fe Mössbauer parameters are collected in Table 4. The spectrum recorded at 298 K was best fitted to two quadrupole split absorptions. The doublet with chemical isomer shift $\delta = 0.30$ mm/s is characteristic of Fe^{3+}. The magnitude of the quadrupole splitting, $\Delta = 0.83$ mm/s, would indicate a distortion of the octahedral array of oxygen ions around iron. The chemical isomer shift of the other doublet, $\delta = 0.28$ mm/s, is intermediate between that characteristic of Fe^{3+} and Fe^{4+} and,

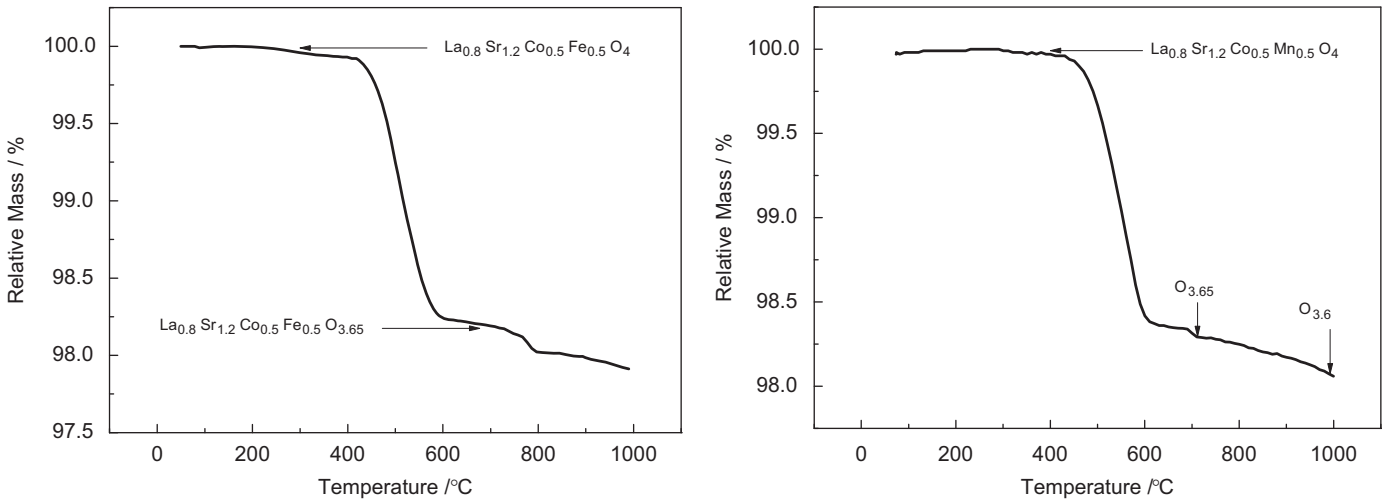

Fig. 2. TG data for the reduction of as-prepared materials using 10% H_2 in N_2.

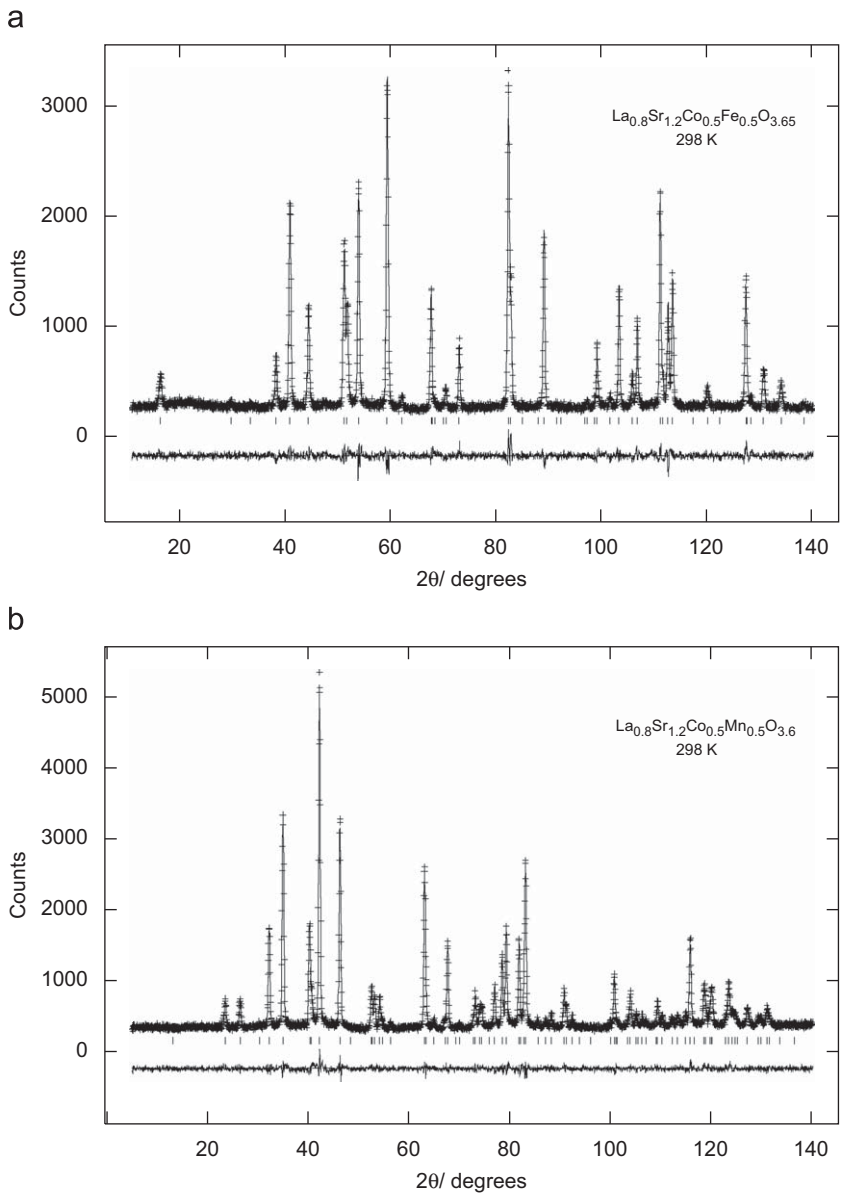

Fig. 3. Observed, calculated and difference plots for the Rietveld profile refinement of NPD data collected from the reduced samples at room temperature.

given the oxygen stoichiometry, we associate this with charge sharing between neighbouring Fe^{3+} and Fe^{4+} ions with a timescale smaller than 10^{-8} s.

The spectrum recorded at 16 K was characterized by a complex broad lined magnetic hyperfine pattern which was best fitted to two discrete sextets ($H = 45.4$ and 41.1 T) and a distribution of magnetic hyperfine fields ($H = 33.9$ T). The large quadrupole interactions associated with the discrete sextets are indicative of a distorted octahedral array of oxygen around iron and is consistent with the large quadrupole splitting observed at 298 K for the Fe^{3+} component. We would associate the overall complexity of the spectrum with the occurrence of complex magnetic interactions between Fe^{3+}, Fe^{4+}, Co^{3+} and Co^{4+}.

The ^{57}Fe Mössbauer spectra recorded from $La_{0.8}Sr_{1.2}Co_{0.5}Fe_{0.5}O_{3.65}$ are shown in Fig. 4b. The spectrum recorded at 298 K was composed of a single doublet with chemical isomer shift $\delta = 0.31$ mm/s characteristic of Fe^{3+}. The large quadrupole splitting ($\Delta = 1.43$ mm/s) is indicative of the Fe^{3+} ion being located in less than six-fold coordination. The spectrum recorded at 16 K showed a single magnetic hyperfine pattern with parameters (Table 4) compatible with this situation.

Table 2
Structural results for the refinement of the NPD data collected from reduced at room temperature.

Atom	x	y	z	$100\times$ Uiso (Å^2)	Occupancy	Site symmetry
$La_{0.8}Sr_{1.2}Co_{0.5}Fe_{0.5}O_{3.65}$, space group $I4/mmm$						
Co/Fe	0	0	0	0.81(7)	0.5/0.5	2*a*
La/Sr	0	0	0.3551(1)	0.95(5)	0.4/0.6	4*e*
O1	0.5	0.061(1)	0	1.19(1)	0.417(3)	8*j*
O2	0	0	0.1675(2)	2.14(6)	1	4*e*
$a = 3.7981(1)$ Å; $c = 13.0515(5)$ Å						
$wR_p = 0.059$; $R_p = 0.0467$; $\chi^2 = 1.4$						
$La_{0.8}Sr_{1.2}Co_{0.5}Mn_{0.5}O_{3.6}$, space group $I4/mmm$						
Co/Fe	0	0	0	0.5(3)	0.5/0.5	2*a*
La/Sr	0	0	0.35634(-9)	1.68(3)	0.4/0.6	4*e*
O1	0.5	0.0543(8)	0	1.46(8)	0.400(3)	8*j*
O2	0	0	0.1674(1)	2.97(5)	1	4*e*
$a = 3.79614(6)$ Å; $c = 13.0116(3)$ Å						
$wR_p = 0.052$; $R_p = 0.0412$; $\chi^2 = 1.39$						

Table 3
Selected bond lengths (Å) for the refined phases.

Bond	$La_{0.8}Sr_{1.2}Co_{0.5}Fe_{0.5}O_{3.65}$	$La_{0.8}Sr_{1.2}Co_{0.5}Mn_{0.5}O_{3.6}$
Co/M–O1[a]	1.9132(5)	1.9092(3)
Co/M–O2	2.187(2)	2.178(2)
La/Sr–O1[a]	2.520(3)	2.521(2)
	2.849(3)	2.815(2)
La/Sr–O2	2.448(3)	2.459(2)
	2.7019(3)	2.7019(2)

[a] Splitting of O1 sites gives twice the number of bonds compared with the ideal site.

3.3. Magnetic characterization

The variation of magnetic susceptibility with temperature for the different samples is shown in Fig. 5. The as-prepared materials generally showed higher magnetization than the reduced ones, with a paramagnetic enhancement of susceptibility at low temperatures. A distinct divergence between ZFC and FC susceptibilities is indicative of spin glass behaviour. As shown in the inset of Fig. 5a, the susceptibility of $La_{0.8}Sr_{1.2}Co_{0.5}Fe_{0.5}O_{3.65}$ shows a well defined maximum at 195 °C, indicating antiferromagnetic (AFM) ordering in this material. NPD data collected from this material at 1.5 K were used to confirm magnetic order at this temperature. A series of

Table 4
^{57}Fe Mössbauer parameters.

Material	Temperature of measurement	$\delta \pm 0.04$ (mm/s)	Δ or $e^2Qq/2 \pm 0.04$ (mm/s)	$H \pm 0.05$ (T)	Area $\pm 3\%$
$La_{0.8}Sr_{1.2}Co_{0.5}Fe_{0.5}O_4$	298	0.30	0.83		45
		0.28	0.38		55
	16	0.42	−0.32	45.4	22
		0.44	−0.26	41.1	28
		0.41	−0.14	33.9	50
$La_{0.8}Sr_{1.2}Co_{0.5}Fe_{0.5}O_{3.65}$	298	0.31	1.43		100
	16	0.44	−0.64	50.1	100

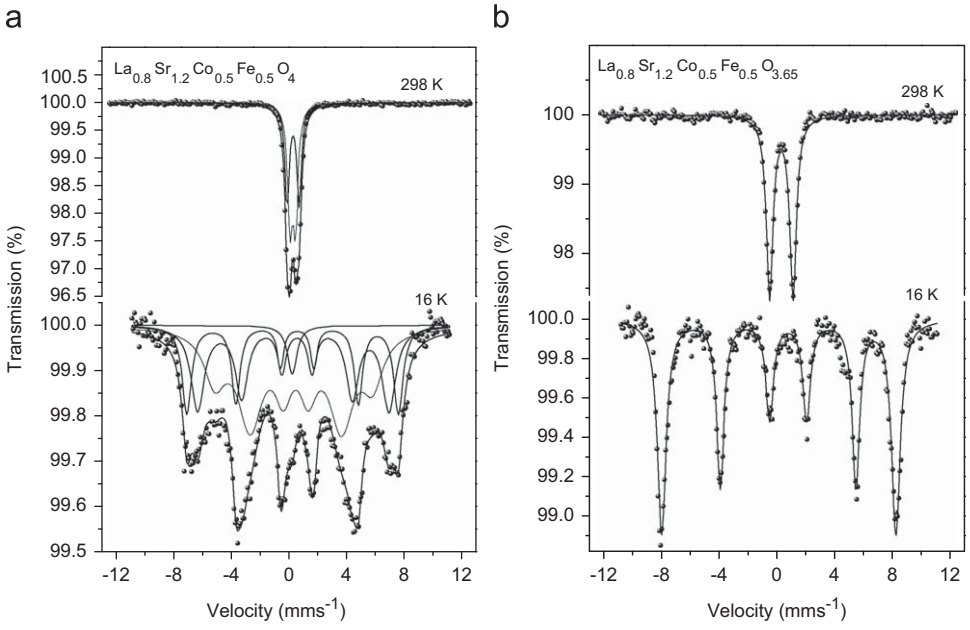

Fig. 4. ^{57}Fe Mössbauer spectra recorded from $La_{0.8}Sr_{1.2}Co_{0.5}Fe_{0.5}O_4$ and $La_{0.8}Sr_{1.2}Co_{0.5}Fe_{0.5}O_{3.65}$ at 298 and 16 K.

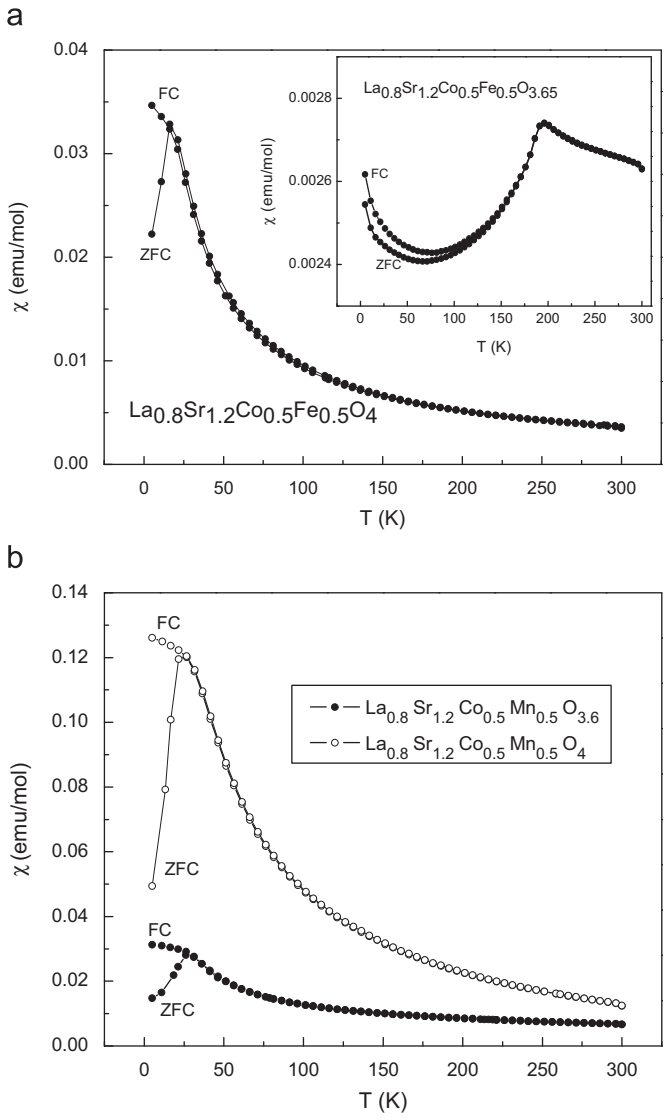

Fig. 5. Variation of magnetic susceptibility (ZFC and FC) with temperature.

additional Bragg reflections, compared with the data sets collected at room temperature, were clearly observed in the low temperature data (see Fig. 6). The low temperature diffraction data showed no evidence of symmetry lowering from tetragonal to orthorhombic, and the magnetic reflections were indexed on a primitive tetragonal cell with lattice parameters $a' = \sqrt{2}a$ and $c' = c$. A strong magnetic peak at $2\theta \sim 20^\circ$ (see Fig. 6), which corresponds to the (100) reflection of the magnetic supercell, indicates the ferromagnetic (FM) component of the moments to be perpendicular to the $\langle 100 \rangle$ directions, and is therefore consistent with noncollinear magnetic order [9,10] previously reported, for example, for $La_{1+x}Sr_{1-x}Co_{0.5}Fe_{0.5}O_{4-\delta}$ [5] (Fig. 7). The profile fit and structural results of the

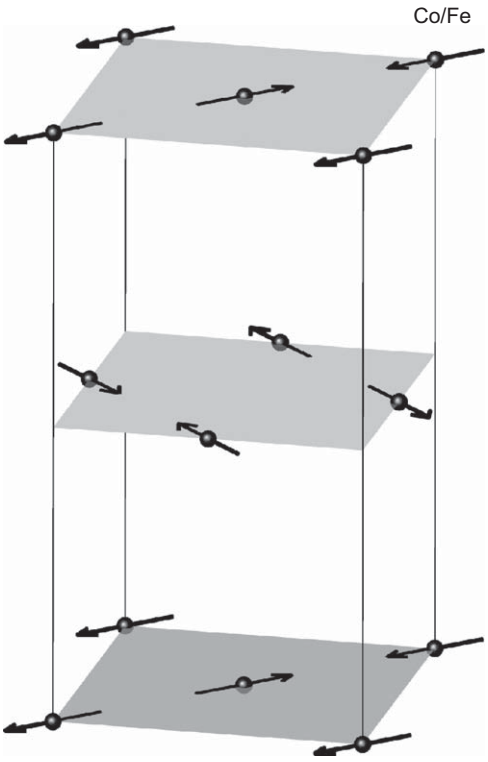

Fig. 7. Magnetic structure of $La_{0.8}Sr_{1.2}Co_{0.5}Fe_{0.5}O_{3.65}$. Only Co/Fe atoms are shown. The arrows indicate the direction of Co/Fe magnetic moments.

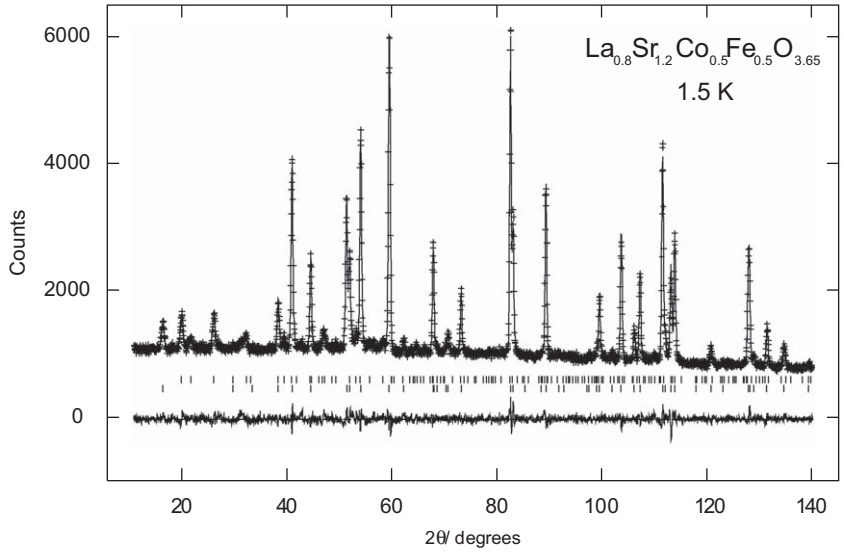

Fig. 6. Observed, calculated and difference NPD profiles collected at 1.5 K from $La_{0.8}Sr_{1.2}Co_{0.5}Fe_{0.5}O_{3.65}$ showing nuclear (lower tick marks) and magnetic (upper tick marks) reflections.

Table 5
Structural results for the refinement of the NPD data collected from $La_{0.8}Sr_{1.2}Co_{0.5}Fe_{0.5}O_{3.65}$ at 1.5 K.

Atom	x	y	z	100 × Uiso (Å^2)	Occupancy	Site symmetry	Bond	Bond length (Å)
$La_{0.8}Sr_{1.2}Co_{0.5}Fe_{0.5}O_{3.65}$, space groups $I4/mmm$ (nuclear) and $P4_2/nn'm$ (magnetic)								
Co/Fe	0	0	0	0.85(9)	0.5	2*a*	Co/Mn–O1[a]	1.9108(5)
La/Sr	0	0	0.3556(1)	0.89(7)	0.6	4*e*	Co/Mn–O2	2.171(2)
O1	0.5	0.064(1)	0	1.02(1)	0.415(4)	8*j*	La/Sr–O1[a]	2.503(3)
O2	0	0	0.1668(2)	1.87(7)	1	4*e*		2.847(3)
$a = 3.79067(5)$ Å; $c = 13.0133(2)$ Å							La/Sr–O2	2.456(3)
								2.6962(3)

Atom	x	y	z	M_x/μ_B	M_y/μ_B	M_z/μ_B	$\|M\|/\mu_B$
Co/Fe	0	*0*	0	2.35(4)	2.35(4)	0	3.33(5)
$wR_p = 0.0366$; $R_p = 0.0289$; $\chi^2 = 1.715$							

[a] Splitting of O1 sites gives twice the number of bonds compared with the ideal site.

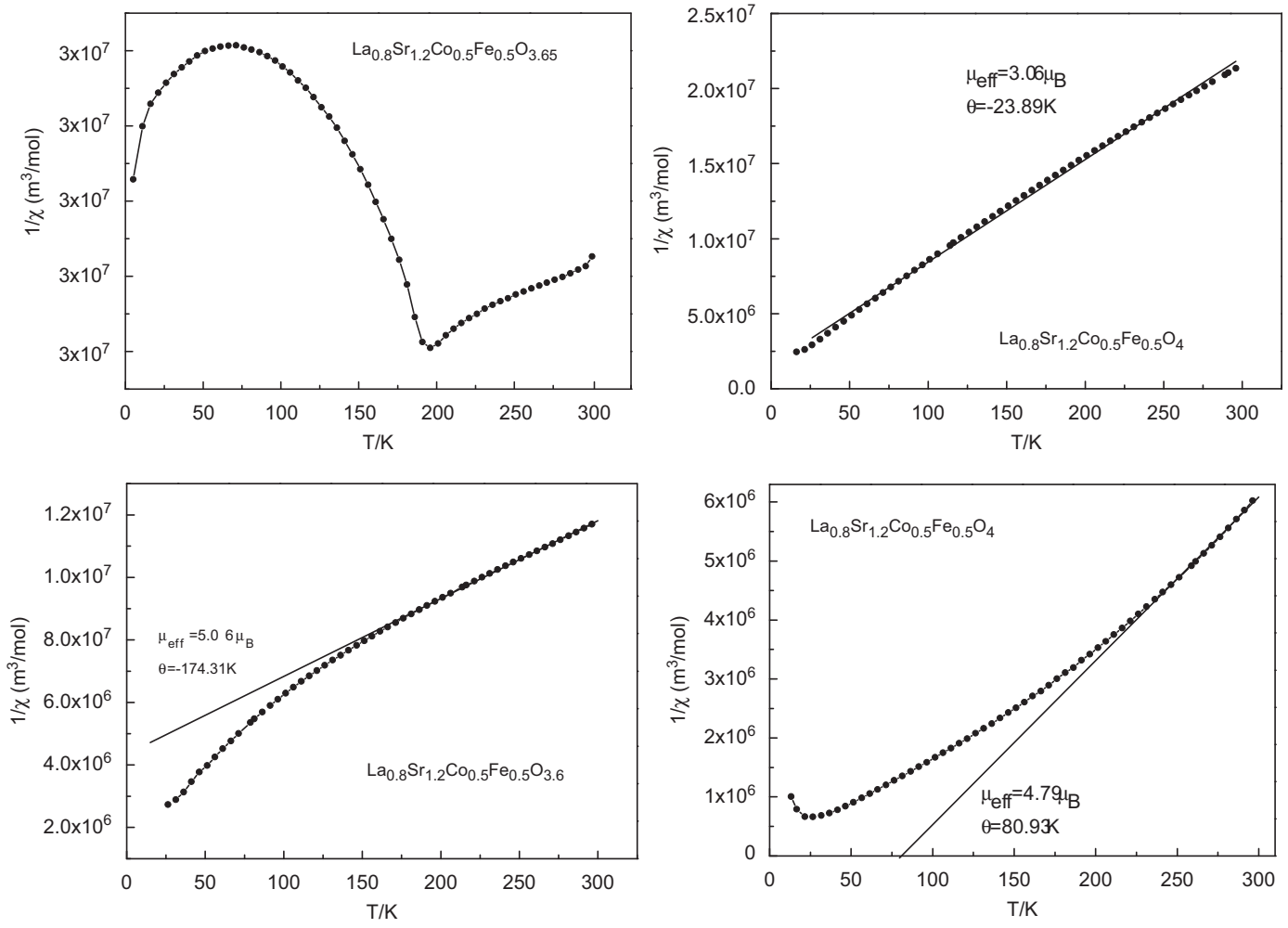

Fig. 8. Variation of the inverse magnetic susceptibilities (ZFC) with temperature.

Rietveld analysis of the low temperature NPD data are shown in Fig. 6 and Table 5, respectively. No evidence of long-range AFM ordering was observed in the low temperature data recorded from $La_{0.8}Sr_{1.2}Co_{0.5}Fe_{0.5}O_4$. The low temperature NPD data confirmed the absence of long-range magnetic order in the manganese-containing samples.

Plots of inverse susceptibility against temperature for the materials studied are shown in Fig. 8. For $La_{0.8}Sr_{1.2}Co_{0.5}Fe_{0.5}O_{3.65}$, the limited temperature range above T_N precluded any fitting of the data; however, for $La_{0.8}Sr_{1.2}Co_{0.5}Fe_{0.5}O_4$, the behaviour is close to Curie–Weiss in nature with $\theta = -24$ K and $\mu_{eff} = 3.06\,\mu_B$. For $La_{0.8}Sr_{1.2}Co_{0.5}Mn_{0.5}O_{3.6}$, the $1/\chi$ versus T plot shows an increased gradient at low temperature which is consistent with magnetic frustration [11]. The application of the Curie–Weiss law for $T > 200$ K gives an effective moment of $5.06\,\mu_B$ and $\theta = -174$ K, consistent with predominantly AFM interactions. Data for

$La_{0.8}Sr_{1.2}Co_{0.5}Mn_{0.5}O_4$ with $T>200$ K imply $\mu_{eff}=4.79\,\mu_B$ and $\theta=81$ K, suggesting mainly ferromagnetic interactions.

4. Discussion

The overall stoichiometries of the materials were determined by NPD and TG analyses as $La_{0.8}Sr_{1.2}Co_{0.5}Fe_{0.5}O_4$, $La_{0.8}Sr_{1.2}Co_{0.5}Mn_{0.5}O_4$ and $La_{0.8}Sr_{1.2}Co_{0.5}Fe_{0.5}O_{3.65}$, $La_{0.8}Sr_{1.2}Co_{0.5}Mn_{0.5}O_{3.6}$ for as-prepared and reduced materials, respectively. Mössbauer spectroscopy confirmed that iron exists in $La_{0.8}Sr_{1.2}Co_{0.5}Fe_{0.5}O_{3.65}$ as Fe^{3+} which suggests the divalent state of cobalt (Co^{2+}) in this material. This material shows long-range AFM magnetic ordering below 195 K which can be readily explained by the presence of Co^{2+} ($t_{2g}^5\,e_g^2$) and Fe^{3+} ($t_{2g}^3\,e_g^2$), for which AFM exchange is expected for all 180° superexchange interactions. The magnetic order has been investigated by low temperature NPD and the ordering scheme shown in Fig. 7 used to account for coupling between Fe^{3+}/Co^{2+} spins. The model suggests a refined moment of $3.33(5)\,\mu_B$ for Fe^{3+}/Co^{2+}, where an average form factor of Fe^{3+} and Co^{2+} was used. The moment is lower than the expected moments for a mixture of high-spin Fe^{3+} and Co^{2+} due to covalence, the low dimensionality of the magnetic order and quantum mechanical effects. Similar effects have been observed previously in $La_{1+x}Sr_{1-x}Co_{0.5}Fe_{0.5}O_{4-\delta}$ [5].

$La_{0.8}Sr_{1.2}Co_{0.5}Fe_{0.5}O_4$, on the other hand, exhibits near Curie–Weiss behaviour with a negative θ value which indicates AFM interactions. The material contains a mixture of M^{3+} and M^{4+} ions; the oxygen stoichiometry suggests the presence of ca. 20% M^{4+} which is not inconsistent with Mössbauer data which implies the presence of some Co^{4+} in this material. Co^{3+}–Fe^{3+} magnetic interactions have been shown in related materials [5] to be ferromagnetic with Co^{3+} in the low-spin state. The relatively low moment calculated from the Curie–Weiss law ($3.06\,\mu_B$) also suggests a low-spin state of Co^{3+} in $La_{0.8}Sr_{1.2}Co_{0.5}Fe_{0.5}O_4$. The complexity of the Mössbauer data of this material at 16 K is consistent with a spin glass state at this temperature (see Fig. 5) and is indicative of complex magnetic interactions between Fe^{3+}, Co^{3+}, Fe^{4+} and Co^{4+}.

The oxygen stoichiometry in $La_{0.8}Sr_{1.2}Co_{0.5}Mn_{0.5}O_4$ suggests a combination of oxidation states ($Co^{3+}/Mn^{3+}+M^{4+}$) or ($Co^{2+}/Mn^{4+}+Co^{3+}$), although the latter is chemically unlikely. However, in the three-dimensional perovskite $LaCo_{0.5}Mn_{0.5}O_3$ [12], an ordered Co^{2+}/Mn^{4+} state is reported. No cation order is observed in $La_{0.8}Sr_{1.2}Co_{0.5}Mn_{0.5}O_4$ and the oxidation state combination ($Co^{3+}/Mn^{3+}+M^{4+}$) is preferred, with 20% of the ions being M^{4+} as suggested by the oxygen stoichiometry. The reduction behaviour of this material (see Fig. 2) suggests reduction of M^{4+} to M^{3+} followed by reduction of Co^{3+} into Co^{2+} to reach the stoichiometry $La_{0.8}Sr_{1.2}Co_{0.5}Mn_{0.5}O_{3.65}$ at 700 °C. Karen et al. [13] have suggested that the Co^{2+}/Mn^{3+} state is more electrochemically favoured than the Co^{3+}/Mn^{2+} state, which supports the reduction of Co^{3+} to Co^{2+} rather than reduction of Mn^{3+} to Mn^{2+}. This behaviour is also consistent with the behaviour of cobalt in iron-containing systems [5]. Further slow reduction as temperature increases suggests partial reduction of Mn^{3+} into Mn^{2+} in $La_{0.8}Sr_{1.2}Co_{0.5}Mn_{0.5}O_{3.6}$; the oxygen stoichiometry suggests that 20% of Mn^{3+} is reduced to Mn^{2+}. $La_{0.8}Sr_{1.2}Co_{0.5}Mn_{0.5}O_{3.6}$ is a spin glass antiferromagnet. This behaviour can be attributed to competing FM and AFM interactions between high-spin Co^{2+}, Mn^{3+} and Mn^{2+}. The effective moment observed at $T>200$ K ($5.06\,\mu_B$) is in good agreement with the theoretical spin-only value corresponding to high-spin Co^{2+}, Mn^{3+} and Mn^{2+} ($5.01\,\mu_B$). It is likely that competing FM and AFM interactions account for the spin glass state observed in case of $La_{0.8}Sr_{1.2}Co_{0.5}Mn_{0.5}O_4$ which may correspond to competing AFM and FM interactions between Co^{3+}, Mn^{3+} and M^{4+} ions. The uncertain nature of the cation oxidation states makes it difficult to interpret the observed effective magnetic moment of $4.79\,\mu_B$.

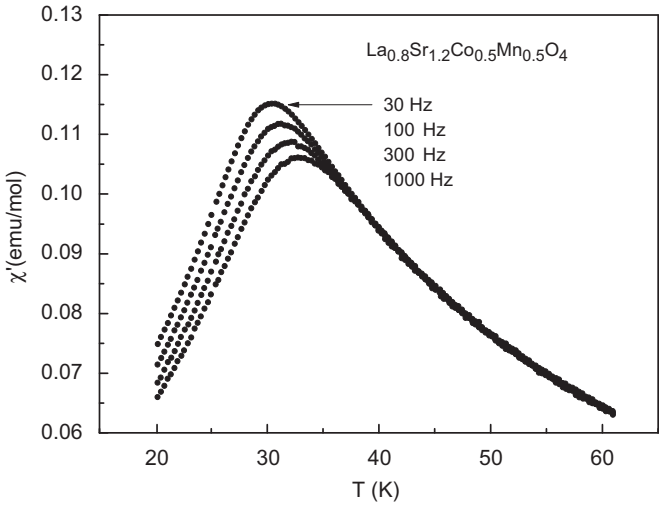

Fig. 9. Plot of real component (χ') of ac susceptibility versus temperature for $La_{0.8}Sr_{1.2}Co_{0.5}Mn_{0.5}O_4$.

The spin glass behaviour has been confirmed by ac magnetic susceptibility measurements. The frequency dependence of the ac magnetic susceptibility of $La_{0.8}Sr_{1.2}Co_{0.5}Mn_{0.5}O_4$, for example, is shown in Fig. 9. The data clearly show that the location of the cusp at the freezing temperature is dependent on the frequency of the ac susceptibility measurement which is a characteristic feature of spin glasses.

TG and NPD data indicate that $La_{0.8}Sr_{1.2}Co_{0.5}Mn_{0.5}O_4$ withstands reducing conditions (10% H_2/N_2) up to 1000 °C with retention of structural stability and crystal symmetry. Large oxygen nonstoichiometry along with the structural stability at high temperature in reducing environments suggests a possible use for this material in applications such as oxygen separation membranes.

The reduced materials are formed via deintercalation of oxygen from the equatorial sites of the K_2NiF_4-type structure. Oxygen stoichiometries in these materials suggest the formation of unusual MO_x coordination polyhedra with $x<6$. All polyhedra exhibit elongation parallel to the c axis (M–O2/M–O1 = 1.14 for both samples). These results are consistent with the large quadrupole splitting ($\Delta=1.43$ mm/s) observed in the Mössbauer spectrum recorded from $La_{0.8}Sr_{1.2}Co_{0.5}Fe_{0.5}O_{3.65}$. It might be worth mentioning that formation of oxygen-deficient compounds have been commonly observed in Co-containing perovskite-type materials with layered structure [5,9,14–16], and a variety of unusual geometries with coordination number less than six have been assigned to *B*-site ions in these systems.

Under reduction, an expansion in c occurs as a result of MO_x expansion due to reduction of low-spin Co^{3+} to high-spin Co^{2+}. However, MO_x expansion in the xy plane is inhibited by a contraction in the La/Sr coordination sphere due to lowering of the coordination number (<9); this usually results in freezing or contraction in a [5,9] (see Table 1). This effect explains the observed displacement of equatorial oxygen O1 in the xy plane in order to maintain M–O1 bond lengths. The displacement moves oxygen atoms from the ideal sites (0.5, 0, 0) to (0.5, y, 0) sites, with y being dependent on the degree of oxygen deficiency. This is clearly observed here, where the y value is 0.061(1) and 0.0543(8) for $La_{0.8}Sr_{1.2}Co_{0.5}Mn_{0.5}O_{3.6}$ and $La_{0.8}Sr_{1.2}Co_{0.5}Fe_{0.5}O_{3.65}$ as compared with 0.0333(7) and 0.0509(6) for $La_{1.2}Sr_{0.8}Co_{0.5}Fe_{0.5}O_{3.85}$ and $LaSrCo_{0.5}Fe_{0.5}O_{3.75}$ [5].

5. Conclusions

The M^{4+}-containing K_2NiF_4-type phases $La_{0.8}Sr_{1.2}Co_{0.5}Fe_{0.5}O_4$ and $La_{0.8}Sr_{1.2}Co_{0.5}Mn_{0.5}O_4$ have been synthesized by a sol–gel technique. The materials are stoichiometric in oxygen and exhibit spin glass behaviour at low temperature due to competing FM and AFM interactions. Under reduction, the oxidation states Co^{2+}/Fe^{3+} and Co^{2+}/Mn^{3+} (Mn^{2+}) were produced in $La_{0.8}Sr_{1.2}Co_{0.5}Fe_{0.5}O_{3.65}$ and $La_{0.8}Sr_{1.2}Co_{0.5}Mn_{0.5}O_{3.6}$, respectively. Oxide ion vacancies are distributed within the equatorial planes of the structure with an associated twisting of MO_x polyhedra around the z axis. Co^{2+} and Fe^{3+} ions couple antiferromagnetically in $La_{0.8}Sr_{1.2}Co_{0.5}Fe_{0.5}O_{3.65}$ with a tetragonal noncollinear order of magnetic moments. A ferromagnetic component of interaction due to the presence of Mn^{3+} in $La_{0.8}Sr_{1.2}Co_{0.5}Mn_{0.5}O_{3.6}$ results in a spin glass state in this material.

Acknowledgments

We thank the Egyptian Education Bureau (London) for financial support (H. El Shinawi). We also thank the EU for financial support for obtaining NPD data, and we are grateful to V. Pomjakushin for assistance with the collection of NPD data.

References

[1] S.J. Skinner, J.A. Kilner, Solid State Ionics 135 (2000) 709–712.
[2] V.V. Vashook, H. Ullman, O.P. Olshevskaya, V.P. Kulik, V.E. Lukashevich, L.V. Kokhanovskii, Solid State Ionics 138 (2000) 99–104.
[3] S.E. Dann, M.T. Weller, D.B. Currie, J. Solid State Chem. 97 (1992) 179–185.
[4] F. Prado, T. Armstrong, A. Caneiro, A. Manthiram, J. Electrochem. Soc. 148 (2001) J7–J14.
[5] H. El Shinawi, C. Greaves, J. Solid State Chem. 181 (2008) 2705–2712.
[6] A.C. Larson, R.B. Von Dreele, General Structural Analysis System, Los Alamos National Laboratory, Los Alamos, NM, 1994.
[7] V.K. Sears, Neutron News 3 (1992) 29.
[8] P.H. Labbe, M. Ledesert, V. Caignaert, B. Raveau, J. Solid State Chem. 91 (1991) 362–369.
[9] M.A. Hayward, M.J. Rosseinsky, Chem. Mater. 12 (2000) 2182–2195.
[10] A.L. Hector, C.S. Knee, A.I. MacDonald, D.J. Price, M.T. Weller, J. Mater. Chem. 15 (2005) 3093–3103.
[11] K.V. Rao, M. Fahnle, E. Figueroa, O. Beckman, L. Hedman, Phys. Rev. B 27 (1983) 3104–3107.
[12] C.L. Bull, D. Gleeson, K.S. Knight, J. Phys. Condens. Matter 15 (2003) 4927–4936.
[13] P. Karen, E. Suard, F. Fauth, P.M. Woodward, Solid State Sci. 6 (2004) 1195–1204.
[14] J.M. Hill, B. Dabrowski, J.F. Mitchell, J.D. Jorgensen, Phys. Rev. B 74 (2006) 174417.
[15] Y. Bréard, C. Michel, M. Hervieu, F. Studer, A. Maignan, B.B. Raveau, Chem. Mater. 14 (2002) 3128–3135.
[16] A. Bowman, M. Allix, D. Pelloquin, M.J. Rosseinsky, J. Am. Chem. Soc. 128 (2006) 12606–12607.